EUROPEAN ORGANIZATION FOR NUCLEAR RESEARCH

CERN–EP/98-86
May 22, 1998

A next-to-leading order QCD analysis of the spin structure function g_1

The Spin Muon Collaboration (SMC)

Abstract

We present a next-to-leading order QCD analysis of the presently available data on the spin structure function g_1 including the final data from the Spin Muon Collaboration (SMC). We present results for the first moments of the proton, deuteron and neutron structure functions, and determine singlet and non-singlet parton distributions in two factorization schemes. We also test the Bjorken sum rule and find agreement with the theoretical prediction at the level of 10%.

Submitted to Physical Review D

B. Adeva[18], T. Akdogan[2], E. Arik[2], B. Badelek[21,23], G. Bardin[17,y], G. Baum[1], P. Berglund[8], L. Betev[13], R. Birsa[20], N. de Botton[17], F. Bradamante[20], A. Bravar[11], A. Bressan[20,n], S. Bültmann[1,b], E. Burtin[17], D. Crabb[22], J. Cranshaw[20], T. Çuhadar[2,15], S. Dalla Torre[20], R. van Dantzig[15], B. Derro[4], A. Deshpande[24], S. Dhawan[24], C. Dulya[15,4,c], S. Eichblatt[d], D. Fasching[16,e], F. Feinstein[17], C. Fernandez[18,9], S. Forthmann[7], B. Frois[17], A. Gallas[18], J.A. Garzon[18,9], H. Gilly[6], M. Giorgi[20], E. von Goeler[o], S. Goertz[3], G. Gracia[18,f], N. de Groot[15,g], M. Grosse Perdekamp[24,w], K. Haft[13], D. von Harrach[11], T. Hasegawa[14,h], P. Hautle[5,i], N. Hayashi[14,j], C.A. Heusch[5,k], N. Horikawa[14], V.W. Hughes[24], G. Igo[4], S. Ishimoto[14,l], T. Iwata[14], E.M. Kabuß[11], T. Kageya[14,m], A. Karev[10], H.J. Kessler[6,v], T.J. Ketel[15], J. Kiryluk[23], Yu. Kisselev[10], D. Krämer[1], V. Krivokhijine[10], W. Kröger[5,k], V. Kukhtin[10], K. Kurek[23], J. Kyynäräinen[1,8], M. Lamanna[20], U. Landgraf[6], J.M. Le Goff[17], F. Lehar[17], A. de Lesquen[17], J. Lichtenstadt[19], M. Litmaath[15,n], A. Magnon[17], G.K. Mallot[11]n, F. Marie[17], A. Martin[20], J. Martino[17], T. Matsuda[14,h], B. Mayes[9], J.S. McCarthy[22], K. Medved[10], W. Meyer[3], G. van Middelkoop[15], D. Miller[16], Y. Miyachi[14], K. Mori[14], J. Moromisato[o], J. Nassalski[23], L. Naumann[5,†], T.O. Niinikoski[5], J.E.J. Oberski[15], A. Ogawa[14,p], C. Ozben[2], H. Pereira[17], F. Perrot-Kunne[17], D. Peshekhonov[10], R. Piegia[5,r] L. Pinsky[9], S. Platchkov[17], M. Plo[18], D. Pose[10], H. Postma[15], J. Pretz[11,x], R. Puntaferro[20], G. Rädel[5], A. Rijllart[5], G. Reicherz[3], J. Roberts[q] M. Rodriguez[21,r], E. Rondio[23,5], I. Sabo[19], J. Saborido[18], A. Sandacz[23], I. Savin[10], P. Schiavon[20], A. Schiller[7], E. P. Sichtermann[15], F. Simeoni[20], G.I. Smirnov[10], A. Staude[13], A. Steinmetz[11,13], U. Stiegler[5], H. Stuhrmann[7], M. Szleper[23], F. Tessarotto[20], D. Thers[17], W. Tlaczala[23,s], A. Tripet[1], G. Unel[2], M. Velasco[16,n], J. Vogt[13], R. Voss[5], C. Whitten[4], R. Windmolders[12], R. Willumeit[7], W. Wislicki[23], A. Witzmann[6,t], J. Ylöstalo[8], A.M. Zanetti[20], K. Zaremba[23,s], J. Zhao[7,u]

[1] University of Bielefeld, Physics Department, 33501 Bielefeld, Germany
[2] Bogaziçi University and Istanbul Technical University, Istanbul, Turkey
[3] University of Bochum, Physics Department, 44780 Bochum, Germany
[4] University of California, Department of Physics, Los Angeles, 90024 CA, USA
[5] CERN, 1211 Geneva 23, Switzerland
[6] University of Freiburg, Physics Department, 79104 Freiburg, Germany
[7] GKSS, 21494 Geesthacht, Germany
[8] Helsinki University of Technology, Low Temperature Laboratory and Institute of Particle Physics Technology, Espoo, Finland
[9] University of Houston, Department of Physics, Houston, 77204-5506 TX, USA
[10] JINR, Dubna, RU-141980 Dubna, Russia
[11] University of Mainz, Institute for Nuclear Physics, 55099 Mainz, Germany
[12] University of Mons, Faculty of Science, 7000 Mons, Belgium
[13] University of Munich, Physics Department, 80799 Munich, Germany
[14] Nagoya University, CIRSE and Department of Physics, Furo-Cho, Chikusa-Ku, 464 Nagoya, Japan
[15] NIKHEF, Delft University of Technology, FOM and Free University, 1009 AJ Amsterdam, The Netherlands
[16] Northwestern University, Department of Physics, Evanston, 60208 IL, USA
[17] C.E.A. Saclay, DAPNIA, 91191 Gif-sur-Yvette, France
[18] University of Santiago, Department of Particle Physics, 15706 Santiago de Compostela, Spain
[19] Tel Aviv University, School of Physics, 69978 Tel Aviv, Israel
[20] INFN Trieste and University of Trieste, Department of Physics, 34127 Trieste, Italy
[21] Uppsala University, Department of Radiation Sciences, 75121 Uppsala, Sweden
[22] University of Virginia, Department of Physics, Charlottesville, 22901 VA, USA
[23] Soltan Institute for Nuclear Studies and Warsaw University, 00681 Warsaw, Poland
[24] Yale University, Department of Physics, New Haven, 06511 CT, USA
[b] Now at University of Virginia, Department of Physics, Charlottesville, 22901 VA, USA
[c] Now at CIEMAT, Avda Complutense 22, 28040, Madrid, Spain
[d] Now at Fermi National Accelerator Laboratory, Batavia, 60510 IL, USA
[e] Now at University of Wisconsin, USA
[f] Now at NIKHEF P.O.B. 41882, 1009 DB Amsterdam, The Netherlands
[g] Now at SLAC, Stanford 94309 CA USA
[h] Permanent address: Miyazaki University, Faculty of Engineering, 889-21 Miyazaki-Shi, Japan
[i] Permanent address: Paul Scherrer Institut, 5232 Villigen, Switzerland
[j] Permanent address: The Institute of Physical and Chemical Research (RIKEN), Wako 351-01, Japan
[k] Permanent address: University of California, Institute of Particle Physics, Santa Cruz, 95064 CA, USA
[l] Permanent address: KEK, Tsukuba-Shi, 305 Ibaraki-Ken,Japan
[m] Now at University of Michigan, Ann Arbor MI48109, USA
[n] Now at CERN, 1211 Geneva 23, Switzerland
[o] Permanent address: Northeastern University, Department of Physics, Boston, 02115 MA, USA
[p] Now at Penn. State University, 303 Osmond Lab, University Park, 16802 PA, USA
[q] Permanent address: Rice University, Bonner Laboratory, Houston, TX 77251-1892, USA
[r] Permanent address: University of Buenos Aires, Physics Department, 1428 Buenos Aires, Argentina
[s] Permanent address: Warsaw University of Technology, Warsaw, Poland
[t] Now at F.Hoffmann-La Roche Ltd., CH-4070 Basel, Switzerland

1 Introduction

We present a perturbative QCD (pQCD) analysis in next-to-leading order (NLO) of the world data on polarized lepton-nucleon deep inelastic scattering (DIS). The data used in this analysis include the final results [1] presented by the Spin Muon Collaboration (SMC). From the world data we determine the first moments of the polarized structure functions.

The accuracy of the experimental data on the polarized structure function $g_1(x)$ has improved significantly in the past few years. All experiments have confirmed the small values of the first moments of g_1 of the nucleon, thus confirming the violation of the Ellis-Jaffe spin sum rule [2] and the small contribution of quark spins to the nucleon spin (a_0 in the naive quark parton model). Motivated by the availability of accurate experimental data, theoretical tools to analyze them have been advanced, e.g. NLO calculations in pQCD for the spin structure functions. The nucleon spin can now be separated into some of its components in the framework of pQCD. Of special interest is the role played by the polarized gluon distribution. It has been suggested [3] that if the polarized gluon distribution is found to be significant, it could explain the small value of the quark contribution to the proton spin.

The Bjorken sum rule [4] is a relation between the first moments of the spin structure functions of proton and neutron. It is a fundamental result of QCD first derived using current algebra. Most experimental efforts in the past have been oriented towards the direct confirmation of this relation. The determinations of the first moments from the experimental data depended on extrapolations due to the limited kinematic range of the experiments. In this paper we address this issue within the framework of pQCD: we first present a pQCD analysis of the world data assuming the Bjorken sum rule to be valid, and discuss the uncertainties in the analysis and their origins. We then release the Bjorken sum constraint and check if the available data and the theoretical framework of pQCD allow a test of the Bjorken sum rule.

A number of theoretical papers have been published on this topic over the last few years [5, 6, 7, 8]. The E154 collaboration has recently presented their pQCD analysis of the data [9]. The SMC has published results in which the pQCD analysis was used to evaluate the first moments $\Gamma_1^{p,d,n}$ at a fixed Q^2 [10, 11, 12], but a detailed description of the procedure of the pQCD analysis was not given. We do that in this paper.

In the pQCD analysis, apart from the published data from other collaborations at CERN, SLAC and DESY, we use a new and final set of data [1] from SMC which includes improved values of g_1 at low x obtained by requiring the presence of a high energy hadron in the final state. In addition, an improved value of the beam polarization (w.r.t. our previous publications [10, 11, 12]) was used in the evaluation of the asymmetries. We study the impact of each experimental data set and the sources of theoretical uncertainties on the first moments of the spin structure functions and on the polarized parton distributions.

In section 2, after a brief overview of the theoretical framework needed for the pQCD analysis, we describe the method used. We performed this analysis using two different mathematical approaches and computer codes. With the improved data available today, we determine the polarized parton distributions and study their stability. A comparison

[u] Now at Los Alamos National Laboratory, Los Alamos, NM 87545, USA
[v] Now at SBC Warburg Dillon Read, CH-4002 Basel, Switzerland
[w] Now at University of Mainz, Institute of Nuclear Physics, 55099, Germany
[x] Now at Physics Department, Yale University, New Haven CT 06520
[y] deceased

of results obtained in the two programs allows us to do this. We discuss the main features of the two programs used for calculating the Q^2 evolution emphasizing their differences and similarities, and compare the results obtained. The choice of the factorization scheme has been discussed extensively in [6, 15]. It has been shown analytically that the choice is arbitrary, and that one can translate results from one scheme to the other. We chose two widely used schemes in the field of polarized DIS and present results based on world data in those two schemes. Recently, theoretical [8] as well as experimental [9] collaborations have presented results on the determination of the strong coupling constant α_s using pQCD analyses of the spin structure function data. We present our result and comment on it. Towards the end of section 2 we discuss in detail the experimental systematic and theoretical sources that contribute to the total uncertainty in the polarized parton distribution functions (PDF).

Section 3 discusses the results, namely the first moments of the spin structure functions, the quark and gluon parton distribution functions, and the evaluation of the Bjorken sum rule. We present two evaluations of the Bjorken sum rule: one from the QCD fit in NLO and another from a fit restricted to the non-singlet part of the spin structure function.

2 The QCD Analysis - Procedure and Uncertainty Estimation

2.1 Introduction: Experimental Measurement of g_1

In polarized DIS experiments the asymmetry, $A_\parallel$, of the cross sections for parallel and antiparallel orientations of the beam and target spins,

$$A_\parallel = \frac{\sigma^{\uparrow\downarrow} - \sigma^{\uparrow\uparrow}}{\sigma^{\uparrow\downarrow} + \sigma^{\uparrow\uparrow}} \tag{1}$$

is measured. The evaluation of the asymmetry, $A_\parallel$, requires knowledge of the incident beam and target polarizations, and of the dilution factor which accounts for the fact that only a fraction of the target nucleons is polarizable. The asymmetry, $A_\parallel$, and the spin-dependent structure function, g_1, are related to the virtual photon-nucleon asymmetries, A_1 and A_2, [16] by

$$A_\parallel = D(A_1 + \eta A_2), \qquad\qquad g_1 = \frac{F_2}{2x(1+R)}(A_1 + \gamma A_2), \tag{2}$$

in which the factors η and γ depend only on kinematic variables and on the nucleon mass, while the depolarization factor D depends on kinematic variables and the ratio of total photoabsorption cross sections for longitudinally and transversely polarized virtual photons $R = \sigma_{\rm L}/\sigma_{\rm T}$. The structure function g_1 is computed using Eq.(2) and parametrizations for F_2 [1] and R. For $x < 0.12$ a parametrization of R based on the data from Ref. [13] was used, while for $x > 0.12$ the parametrization in Ref. [14] was used. For other experimental aspects of the g_1 measurement see [1, 12].

In the pQCD analysis presented in this paper we use the final SMC proton and deuteron data from [1] with $Q^2 > 1$ GeV^2, the proton data from the EMC [17], the proton and deuteron data from the E143 collaboration [18, 19, 20], and the neutron data from the E142 [21], the E154 [22] and the HERMES [23] collaborations.

As in our previous publications [10], we assume that the deuteron structure function $g_1^{\rm d}$ is related to the proton and neutron structure functions $g_1^{\rm p}$ and $g_1^{\rm n}$ by

$$g_1^{\rm p} + g_1^{\rm n} = \frac{2g_1^{\rm d}}{(1 - \frac{3}{2}\omega_D)}, \tag{3}$$

where $\omega_{\rm D} = 0.05 \pm 0.01$ is the D-wave state probability in the deuteron.

2.2 Theoretical Framework

The structure function g_1 is related to the polarized quark and gluon distributions through

$$\begin{aligned} g_1(x,t) &= \tfrac{1}{2}\langle e^2\rangle \int_x^1 \frac{{\rm d}y}{y}\Big[C_{\rm S}^q(\tfrac{x}{y},\alpha_s(t))\Delta\Sigma(y,t) \\ &+ 2n_f C^g(\tfrac{x}{y},\alpha_s(t))\Delta g(y,t) C_{\rm NS}^q(\tfrac{x}{y},\alpha_s(t))\Delta q_{\rm NS}(y,t)\Big], \end{aligned} \tag{4}$$

where $\langle e^2\rangle = n_f^{-1}\sum_{k=1}^{n_f} e_k^2$ is the average squared quark charge, $t = \ln(Q^2/\Lambda^2)$ where Λ is the QCD scale parameter, $\Delta\Sigma$ and $\Delta q_{\rm NS}$ are the singlet and non-singlet polarized quark distributions

$$\Delta\Sigma(x,t) = \sum_{i=1}^{n_f}\Delta q_i(x,t), \qquad \Delta q_{\rm NS}(x,t) = \sum_{i=1}^{n_f}(e_i^2/\langle e^2\rangle - 1)\Delta q_i(x,t), \tag{5}$$

and $C_{S,NS}^q(\alpha_s(t))$ and $C^g(\alpha_s(t))$ are the quark and gluon coefficient functions. The x and Q^2 dependence of the polarized quark and gluon distributions is given by the DGLAP equations [24],

$$\frac{\rm d}{{\rm d}t}\Delta\Sigma(x,t) = \frac{\alpha_s(t)}{2\pi}\int_x^1 \frac{{\rm d}y}{y}\Big[P_{qq}^{\rm S}(\tfrac{x}{y},\alpha_s(t))\Delta\Sigma(y,t) + 2n_f P_{qg}(\tfrac{x}{y},\alpha_s(t))\Delta g(y,t)\Big], \tag{6}$$

$$\frac{\rm d}{{\rm d}t}\Delta g(x,t) = \frac{\alpha_s(t)}{2\pi}\int_x^1 \frac{{\rm d}y}{y}\Big[P_{gq}(\tfrac{x}{y},\alpha_s(t))\Delta\Sigma(y,t) + P_{gg}(\tfrac{x}{y},\alpha_s(t))\Delta g(y,t)\Big], \tag{7}$$

$$\frac{\rm d}{{\rm d}t}\Delta q_{\rm NS}(x,t) = \frac{\alpha_s(t)}{2\pi}\int_x^1 \frac{{\rm d}y}{y}\,P_{qq}^{\rm NS}(\tfrac{x}{y},\alpha_s(t))\Delta q_{\rm NS}(y,t), \tag{8}$$

where P_{ij} are polarized splitting functions.

The full set of coefficient functions [25] and splitting functions [26] has been computed up to next-to-leading order in α_s. At next-to-leading order the splitting functions, the coefficient functions and in general the parton distributions depend on the renormalization and factorization schemes, while the physical observables, such as g_1, remain scheme-independent. Parton distributions in different schemes can be different but they are related to each other by well-defined transformations [15].

Two widely used schemes in the pQCD analysis of the spin structure function data are the $\overline{\rm MS}$ scheme [27] and the Adler-Bardeen (AB) [6] scheme which is a modified $\overline{\rm MS}$ scheme. In the $\overline{\rm MS}$ scheme the first moment of the gluon coefficient function C^g is equal to zero, which implies that the gluon density $\Delta g(x,Q^2)$ does not contribute to the integral $\Gamma_1 = \int_0^1 g_1(x)dx$ (See Eqn.4). In the AB scheme the axial anomaly ($\sim \alpha_s(Q^2)\Delta g(Q^2)$) contributes explicitly to Γ_1. The first moments of the singlet quark distribution in the two schemes differ by an amount proportional to $\alpha_s\Delta g$:

$$\Delta\Sigma_{\overline{\rm MS}}(Q^2) = \Delta\Sigma_{\rm AB} - n_f\frac{\alpha_s(Q^2)}{2\pi}\Delta g(Q^2) \tag{9}$$

where $\Delta g(Q^2)$ is the value of Δg that one obtains in an analysis performed in the AB scheme. Since at leading order the first moment of the polarized gluon distribution behaves as $1/\alpha_s$, the scheme dependence in Eqn. 9 persists at all Q^2 and is potentially large if the first moment of the gluon distribution is large [3].

2.3 Method of QCD Analysis

Polarized parton distributions are extracted from experimental structure function data in the following way. One needs an initial functional form for the parton distributions at an initial $Q^2 = Q_i^2$. It needs to be flexible enough to allow for the description of the low x as well as the high x behavior of the data and to connect the high and low x behaviors with a minimal number of free parameters. In this spirit we parametrize the initial polarized parton distributions at a starting $Q^2 = Q_i^2$ as

$$\Delta f(x, Q^2) = N(\alpha_f, \beta_f, a_f)\ \eta_f\ x^{\alpha_f}(1-x)^{\beta_f}(1 + a_f\ x), \tag{10}$$

where $N(\alpha, \beta, a)$ is fixed by the normalization condition,

$$N(\alpha, \beta, a) \int_0^1 x^{\alpha}(1-x)^{\beta}(1+ax)dx = 1,$$

and Δf denotes $\Delta\Sigma$, $\Delta q_{\rm NS}$, or Δg. With this normalization the parameters $\eta_g, \eta_{\rm NS}$, and $\eta_{\rm S}$ are the first moments of the gluon, the non-singlet quark and the singlet quark distributions at the starting scale, respectively. We evolve the initial parton distributions to the Q^2 of the data points using Eqs.(6-8) and evaluate g_1 with Eq.(4). We determine a χ^2 using this calculated g_1, $g_1^{\rm calc}(x, Q^2)$, the measured $g_1^{\rm data}(x, Q^2)$, and its statistical uncertainty $\delta_{\rm stat} g_1^{\rm data}(x, Q^2)$ as:

$$\chi^2 = \sum_{i=1}^{n} \frac{\left[g_1^{\rm calc}(x, Q^2) - g_1^{\rm data}(x, Q^2)\right]^2}{(\delta_{\rm stat} g_1^{\rm data}(x, Q^2))^2}. \tag{11}$$

Here n stands for the number of experimental data points used in the pQCD fit. We minimize this χ^2 by changing the initial parton distribution coefficients $\eta_f, \alpha_f, \beta_f$ and a_f to get the best fit parton distribution at the initial Q_i^2. Only statistical errors on the data were used in the fit. Various systematic uncertainties, being correlated, had to be handled separately and will be discussed in Section 2.7. Unless otherwise mentioned we chose the initial scale, $Q_i^2 = 1$ GeV^2. Since most of the experimental data lie in the range $1 < Q^2 < 10$ GeV^2, when it was relevant to study the Q_i^2 dependence of a result, we have done so using $Q_i^2 = 10$ GeV^2 as the upper limit for the initial scale. The normalization of the non-singlet quark densities $\eta_{\rm NS}^{\rm p,n}$ are fixed using the neutron and hyperon β decay constants and assuming SU(3) flavor symmetry: $\eta_{\rm NS}^{\rm p,n} = (\pm)\frac{3}{4}\frac{g_A}{g_V} + \frac{1}{4}a_8$. We use $|g_A/g_V| = F + D = 1.2601 \pm 0.0025$ [28] and $F/D = 0.575 \pm 0.016$ [29]. In the analyses in this paper which test the Bjorken sum rule the value of g_A/g_V will be made a free parameter in the fit. In order to be able to estimate the effect of the yet unknown higher-than-NLO corrections to this analysis, the factorization scale, M^2, and the renormalization scale, μ^2, in this analysis were taken to be of the form $M^2 = k_1 \cdot Q^2$ and $\mu^2 = k_2 \cdot Q^2$ with $k_1 = k_2 = 1$ for the standard fit. The variation in the factors $k_{1,2}$ and its role in the uncertainty estimation is discussed in Section 2.7. The value of $\alpha_s(M_Z^2) = 0.118 \pm 0.003$ [28] was used in the analysis. Some tests were done to study the determination of $\alpha_s(Q^2)$ from the spin structure function data. They will be discussed in Section 2.6.

2.4 Comparison of two QCD Evolution Programs

The pQCD analysis by R. Ball *et al.* [6] has been used in our previous publications [10, 11, 12] for evolving our data from the measured Q^2 to a fixed $Q^2 = Q_0^2$. In

this paper we shall call this "Program 1". Another program for the Q^2 evolution was developed within the SMC [31]. In this paper we shall call this "Program 2". This section comments briefly on the evolution programs 1 and 2. In the next section we present a comparison of results obtained with the two programs in the $\overline{\rm MS}$ scheme. The comparison of results for polarized parton distributions from two different programs allows us to study the reliability and stability of our results.

In program 1 the Mellin transformation of the evolution equation and the coefficient and splitting functions is used. The DGLAP equations are solved in the moment space with the boundary condition of Eq. 10 at an initial scale value of Q_i^2. The inverse Mellin transformation needed to return to (x, Q^2) space is performed numerically. This is CPU intensive and the computation time goes approximately linearly with the number of data points used in the QCD analysis. For further details on this analysis the reader is referred to Ref. [6].

The other evolution program [31] computes the evolution in (x, Q^2) variables on a grid covering the range of the experimental data. Differentials in Q^2 are approximated by finite differences. The convolution integrals which appear in Eqs.(4-8) are evaluated using the exact form of the splitting and coefficient functions and values for the distribution functions interpolated between adjacent grid points. The convolution integrals of a splitting or coefficient function and a general parton distribution then only need to be computed at the initialization stage of the procedure. In addition, because the parton distributions are evaluated numerically, the method imposes no practical restrictions on their functional forms. The computation time rises roughly linearly with the number of nodes along the Q^2 axis and roughly as the square of the number of nodes along the x axis. This approximation of the convolution integrals produces satisfactory results if only 30 nodes are used in x, which leads to a reduction in computation time of more than two orders of magnitude compared to a straightforward numerical integration. The Q^2 region of interest was divided into 100 steps. As a check of the accuracy of the method, the numbers of x and Q^2 points were varied from 30 to 80 and from 100 to 200 respectively without producing any significant change in the results.

2.4.1 Result of the comparison

Figure 1 shows the best fits to the $g_1^{\rm p,d,n}$ data at the measured Q^2 obtained using the two programs in the $\overline{\rm MS}$ factorization scheme and starting the evolution from $Q_i^2 = 1$ GeV^2. Since the data do not constrain the high x coefficient, β_g, for the gluon, it was fixed to 4.0 from QCD sum rules[30] for all analyses in this paper. The coefficients a_f (see Eq. 10) for the gluon and non-singlet parton distribution functions were not used in this comparison and we forced the nonsinglet proton and neutron distributions to have the same coefficients α and β as was done in [6, 8][1)]. Both fits describe the data well. The compatibility of the two programs and the invariance with respect to the initial Q^2 was further tested by repeating the fits with $Q_i^2 = 10$ GeV^2. The parameters for the two sets of fits are given in Table 1. The quark singlet and non-singlet coefficients for the parton distributions are nearly the same in both fits and their parameters are consistently (and well) determined by the two programs. On the contrary, the coefficients of the gluon distribution are poorly determined in both programs, and as such the polarized gluon distribution seems to be only marginally determined by the data. Due to the approximate

[1)] For the purpose of comparison of the programs such constraints and assumptions make no difference, other than reducing the number of free parameters. Later in this paper when we do fits which are used in the evaluation of integrals we release some of these constraints.

scale independence of $(\alpha_s \eta_g)$, since $\alpha_s(Q^2)$ reduces by a factor $\sim$2 between 1 and 10 GeV^2, the first moment η_g is expected to increase by the same factor between the two values of Q^2. The fitted values of η_g are compatible within their large errors.

The parton distributions obtained in the above fits, performed at $Q_i^2 = 1$ and 10 GeV^2 in the $\overline{\rm MS}$ scheme, evolved to a fixed $Q_0^2 = 5$ GeV^2 are shown in Fig. 2. The singlet and non singlet quark distribution functions and their evolution in the two programs are very similar. However, the gluon distributions show differences. Keeping in mind the large uncertainty in the determination of gluon distribution coefficients this is not surprising.

Having performed such tests we conclude that given the accuracy of the presently available data different approaches used in the Q^2 evolution do indeed give consistent results and show similar behaviors as far as the uncertainty estimates are concerned. As mentioned before, an independent paper on the QCD analysis in Program 1 has been published [6]. This program has been used previously in the analysis of SMC data [10, 11, 12] and required minimal modification to study the evolution in the two factorization schemes (AB and $\overline{\rm MS}$). In order to preserve continuity with our previous publications and in view of the fact that the Programs 1 and 2 provide consistent results, from now on we will present results using Program 1 exclusively.

2.5 Comparison of Results in $\overline{\rm MS}$ and AB Schemes

The values of the fitted parameters obtained in the $\overline{\rm MS}$ and AB schemes for the initial $Q_i^2 = 1$ GeV^2 are listed in Table 2. In this comparison we have released the constraint requiring the shape of the nonsinglet parton distribution in the proton and neutron to be the same, i.e. we allow different values of α, β in the $\Delta q_{\rm NS}$ of the proton and neutron. The nearly equal values of the χ^2 show that the data are equally well described by the analyses performed in the two schemes with the input parametrizations of Eq. 10. In other words, the functional form of the initial parton distributions in Eq. 10 is flexible enough to describe the data. We observe in Fig. 3 that the fitted $g_1(x)$ distributions, evolved to the reference $Q_0^2 = 5$ GeV^2, differ very little in the range $0.003 < x < 0.8$ in which spin structure function data are available.

The comparison of the fitted polarized parton distributions (Fig. 4) clearly shows how the two schemes differ in the singlet sector. In the $\overline{\rm MS}$ scheme $\Delta\Sigma$ is constrained by the negative values of $g_1^{\rm d}(x)$ at low x to become negative for $x \lesssim 0.05$. The cross-over, x_0, is determined by the linear term in x ($a_s = -1/x_0$). In the AB scheme, this term is not needed because $\Delta\Sigma$ remains positive over the full range of the data. The polarized gluon distribution is found to be larger in the AB scheme and is shifted to lower values of x compared to that in the $\overline{\rm MS}$ scheme. Differences of the same order between gluon determinations in the two schemes have been reported in a previous analysis [9] by the E154 Collaboration. Within the precision of the data, the first moments of the polarized singlet and gluon distributions obtained in the two schemes are compatible with the relation in Eq. 9 at the Q^2 value of 1 GeV^2.

The principal aim of the experimental collaborations is the measurement of the first moments of spin structure functions $g_1^{\rm p,d,n}$. Since the analyses done in both schemes seem to describe the g_1 data equally well it does not matter which scheme we follow. In the past we have used the AB scheme for our results [10, 11, 12]. In order to keep continuity with those publications we use the AB factorization scheme in this paper for all further analysis. We will call this the standard fit.

2.6 Comments on the Determination of $\alpha_s(Q^2)$

The analysis presented so far starts with the spin-dependent virtual photon-nucleon asymmetries measured by different experiments. We determine from these asymmetries the spin-dependent structure functions g_1 using parametrizations of the unpolarized structure functions F_2 and R. The information on scaling violations from the unpolarized nucleon structure functions F_2 (which are measured with significantly better accuracy compared to g_1), is hence an input to the analysis. These scaling violations have been studied and have led to a determination of the strong coupling constant α_s [32].

Recent pQCD analyses of the spin structure functions g_1 [8, 9] have also derived the value of α_s. However, in the presentation of experimental data we have shown (in Fig. 8 and Fig. 9 of [1]) for different x values that no scaling violations are observed in the spin asymmetries $A_1^{\mathrm{p,d}}$ within the experimental uncertainties.

In spite of this, we make the value of $\alpha_s(M_Z^2)$ (which normally is an input parameter in the pQCD analysis) a free parameter in the fit. Table 3 shows the fitted values and the statistical uncertainties in the parameters at $Q_i^2 = 1$ GeV^2. The values change little in comparison with those presented before in Table 2 for the AB scheme. Estimation of uncertainties due to experimental systematic effects in the data and those of theoretical origins (procedure will be described in Section 2.7) gives

$$\alpha_s(M_Z^2) = 0.121 \pm 0.002(\mathrm{stat}) \pm 0.006(\mathrm{syst.\ \&\ theory}). \tag{12}$$

The value of $\alpha_s(M_Z^2)$ indeed comes out to be consistent with that determined from the pQCD analyses of the unpolarized data. As such, while the determination of α_s is certainly possible using the scaling violations of g_1, with the presently available data on A_1 it is difficult to separate the information on scaling violations due to F_2 and due to A_1. In this paper we henceforth always take the value of the strong coupling constant $\alpha_s(M_Z^2) = 0.118 \pm 0.003$ as given in Ref. [28].

2.7 Evaluation of Uncertainties in the Polarized Parton Distribution Functions

Figure 5 shows the results for the parton distributions and their uncertainties. In the calculation of the χ^2 (Eq.11) only the statistical uncertainty on the data points was used. The uncertainty in the parton distribution due to this is shown (cross hatch) with the parton distribution (bold line in the cross hatch).

To estimate the uncertainty in a parton distribution function due to the experimental systematic errors the following procedure was used. For each data set the experimental systematic uncertainties on A_1 due to all sources (σ^i_{syst}) were added in quadrature to calculate a total systematic uncertainty (σ^T_{syst}) for that data set. The QCD fits were then repeated with input values of asymmetries $A_1 \pm \sigma^T_{\mathrm{syst.}}$. The unpolarized structure function, F_2, and R used to evaluate g_1 from A_1 were shifted to the upper and lower limits of their respective parametrizations to estimate their contribution to the uncertainty. Then these experimental, F_2, and R contributions were added quadratically. The resulting envelopes of uncertainty are shown in Fig.5 (vertically hatched band) as a function of x.

In addition to the statistical and systematic uncertainties a significant source of uncertainty in the parton distribution functions comes from uncertainty in the various input parameters to the pQCD analysis. We call them "theoretical" uncertainties. They include uncertainties in the values of factorization and renormalization scales, the value of α_s, the functional form of the initial parton distribution function, the values of quark mass

thresholds, and the value of g_A/g_V. We evaluated them by varying each of these parameters by their known errors (whenever available). The uncertainties in the factorization and renormalization scales are related to the uncertainty in the result due to the neglect of higher order corrections in the pQCD analysis. This was estimated by independently varying factorization and renormalization scale factors k_1 and k_2 in Section 2.3 by 2 in both directions i.e. $0.5 \leq k_1, k_2 \leq 2.0$. For the standard fit the value of $\alpha_s(M_Z^2) = 0.118$ was used. This value was varied between 0.118 ± 0.003. Another input to our analysis is the assumed functional form of Eq.10, the initial parton distribution function. To evaluate its effect on the results two tests were done. First, we used different combinations of constraints on the parameters α_f, β_f, and a_f in Eq. 10 including also an additional term $b\sqrt{x}$ in the polynomial. If the confidence level of the resulting fit was comparable to that of the best fit, then that functional form was accepted and the result of the fit was considered for estimating the uncertainty due to the functional form of the intial parton distribution. Second, we started at an initial scale Q_i^2 different from 1 GeV^2 and observed how different the resultant parton distributions were when evolved to the same common Q_0^2. The theoretical systematic uncertainty bands were then added in quadrature (as functions of x). The envelopes of such uncertainty as a function of x for singlet and nonsinglet parton distributions are shown in Fig. 5 by the horizontally hatched bands. The dominant uncertainties were due to the uncertainty in the factorization scale M^2, the renormalization scale μ^2, and due to the uncertainty in the assumed functional form of the initial parton distributions.

3 QCD Analysis - Results

3.1 Evaluation of First Moments at Fixed Q_0^2

We use all available data in the kinematic region $Q^2 \geq 1$ GeV^2, $x \geq 0.003$ to evaluate $\Gamma_1 = \int_0^1 g_1(x)\mathrm{d}x$ at a fixed Q^2. Starting from $g_1(x, Q^2)$ at the measured x and Q^2 we obtain g_1 at a fixed Q_0^2 as follows:

$$g_1(x, Q_0^2) = g_1(x, Q^2) + [g_1^{\mathrm{fit}}(x, Q_0^2) - g_1^{\mathrm{fit}}(x, Q^2)], \tag{13}$$

where $g_1^{\mathrm{fit}}(x, Q_0^2)$ and $g_1^{\mathrm{fit}}(x, Q^2)$ are the values of g_1 evaluated at Q_0^2 and Q^2 of the experiment using the fit parameters, respectively[2)]. We choose $Q_0^2 = 5\,\mathrm{GeV}^2$ which is close to the average Q^2 of the world data set used in the analysis. In the measured range, $0.003 < x < 0.8$, the contributions to the first moments of the nucleon structure functions calculated from the data are given in Table 4, column 2. The first uncertainty is statistical, the second is systematic and the third is due to the uncertainty in the Q^2 evolution. The method used for combining different data sets is discussed in Refs. [1, 33, 34]. Figs. 6, 7, 8 and their insets show $xg_1^{\mathrm{p,n,d}}$ respectively as a function of x. The areas under the g_1^{fit} curves are given in Table 4, column 3. The integrals calculated in both ways are very similar.

To estimate the contributions to the first moment from the unmeasured low x ($x < 0.003$) and high x ($x > 0.8$) regions, we integrate over g_1^{fit} calculated at $Q^2 = 5$ GeV^2 using the parameters for the parton distributions. The central values and the uncertainties in the low and high x contributions are given in Table 5. The areas under the QCD fit for $x < 0.003$ in Figs. 6, 7, and 8 and their insets correspond to the low x contribution. The uncertainties in the low and high x integrals are obtained using the same procedure as for the estimation of the uncertainty in the QCD evolution described in Section 2.7.

[2)] From now on the superscript "fit" indicates that the quantity was calculated using the best fit parameters of the QCD fit.

Had we taken the traditional approach [10, 11, 12] of using Regge extrapolation in the low x region and a constant A_1 in the high x unmeasured region (bounded by $A_1 < 1$), we would get results using the present data consistent with those presented in Table 5, but with significantly smaller uncertainties (see [11] for a detailed discussion).

The low x contributions to the first moments quoted in Table 5 rely on the validity of the assumption that the parton distribution functions behave as x^α when $x \to 0$ with the values of α quoted in Table II for the AB scheme. Under this condition $g_1^{\rm p}(x, Q_0^2)$ becomes negative below $x \simeq 0.001$, i.e. slightly below the lowest x data available (Fig.6). The $g_1^{\rm d}(x, Q_0^2)$ becomes negative below $x = 0.02$ (Fig.7), while $g_1^{\rm n}(x, Q_0^2)$ is negative for all x (Fig.8). Other functional behaviors of g_1 at low x ($x < 0.003$) have been investigated. The resulting contributions to the moments were found to be in the range of systematic errors quoted in Table 5.

The uncertainties in $\Gamma_1^{\rm p,d,n}(Q_0^2)$, for $Q_0^2 = 5$ GeV^2 are separated by sources in Table 6. The experiments giving the largest three contributions are listed and the remaining ones are added together in "Other Exp.". The largest three theoretical sources of errors, namely, the factorization and renormalization scales, the value of α_s, and the uncertainty in the form of initial parton distribution functions are also given separately. The rest of the sources like the uncertainties in the quark mass thresholds, the values of the constants g_A/g_V, a_8 etc. are collected as one source and called "Others".

Our best estimate for the first moments $\Gamma_1^{\rm p,d,n}(Q_0^2 = 5$ GeV$^2)$ over the full x range is given in the second column of Table 7. The first uncertainty is statistical and the second is systematic. The third uncertainty is due to the low and high x extrapolation and the Q^2 evolution; they are correlated and are both of theoretical origin. The third column of this table gives the values of the first moments at $Q_0^2 = 10$ GeV^2 using the SMC data in the measured x range.

3.2 Δg and a_0 Determination

3.2.1 $\Delta g(Q_0^2)$ and its evolution

Our analysis performed in the AB scheme using an initial $Q_i^2 = 1$ GeV^2 results in

$$\eta_g = \int_0^1 \Delta g(Q^2 = 1{\rm GeV}^2){\rm d}x = 0.99\ ^{+1.17}_{-0.31}\ ({\rm sta})\ ^{+0.42}_{-0.22}\ ({\rm sys})\ ^{+1.43}_{-0.45}\ ({\rm th}). \qquad (14)$$

The procedure used to estimate the uncertainties was the same as described in Section 2.7. When evolved to 5 and 10 GeV^2 the values of η_g become 1.7 and 2.0 respectively. The analysis indicates that the uncertainty in the measurement of this quantity is large. Very little can be said about this quantity on the basis of the present data. Measurements in which the gluon is involved in the leading order (like the photon-gluon fusion process) are needed, in addition to more precise DIS data on g_1, for an improved determination of η_g.

3.2.2 a_0 determination

The values of the singlet axial current matrix element a_0 determined from the fits are shown in Fig. 9 for values of $Q_i^2 = 1, 4, 7, 10$ GeV^2 in the $\overline{\rm MS}$ and AB schemes. The estimated uncertainty is shown for $Q_i^2 = 1$ GeV^2 only. The uncertainties at higher Q_i^2 are comparable. The solid curve is a calculation for the Q^2 dependence of a_0 based on the best fit performed with $Q_i^2 = 1$ GeV^2 in $\overline{\rm MS}$ scheme. The results obtained in this scheme for higher Q_i^2 values fall consistently on this curve. For $Q^2 > 1$ GeV^2 the Q^2 dependence is weak and is below the sensitivity of the existing data. In the $\overline{\rm MS}$ scheme, a_0 is identified

with the integral η_S of the singlet quark distribution (Table II) while in the AB scheme the gluon contribution must be subtracted :

$$a_0(Q^2) = \eta_{\rm S}^{\rm AB} - n_f \frac{\alpha_s(Q^2)}{2\pi}\eta_g(Q^2). \tag{15}$$

Fig. 9 shows that the world data are good enough to test the above relation. In the AB scheme at $Q_0^2 = 1$ GeV^2 we get $a_0 = 0.23 \pm 0.07(\text{sta}) \pm 0.19(\text{sys})$ while at the same Q_0^2 in the $\overline{\rm MS}$ scheme we get $a_0 = 0.19 \pm 0.05(\text{sta}) \pm 0.04(\text{sys})$. These values are compatible within errors as required for a scheme independent quantity and correspond to about 1/3 of the naive QPM expectation $a_0 = a_8 \simeq 0.58$. The errors in the a_0 determined from the analysis in the AB scheme are larger than those determined in the $\overline{\rm MS}$ scheme because of the correlation introduced by Δg and its uncertainty in the evaluation (see Eq. 15).

The first moments $\Gamma^{\rm p,n,d}$ can also be expressed in terms of the matrix elements a_0, a_3 and a_8 [2]. If exact SU(3) flavor symmetry is assumed for the axial octet current, a_3 and a_8 are given by the coupling constants for neutron and hyperon decays, $a_3 = F + D$ and $a_8 = 3F - D$, respectively. Under this assumption and using the input values quoted in Table 7 we obtain at $Q^2 = 5$ GeV^2 $a_0 = 0.13 \pm 0.17$. This result is consistent with those obtained before (directly from QCD analysis) but note that in the measured x range the same Q^2 evolution has been used in all these results.

It has often been suggested that the difference between the low experimental value of a_0 and its naive QPM prediction could be explained by a large gluon contribution. The value of $\eta_S = 0.38^{+0.03\ +0.03\ +0.03}_{-0.03\ -0.02\ -0.05}$ in the AB scheme (only statistical uncertainty on $\eta_{\rm S}$ is shown in Table II), obtained in this analysis does not support this suggestion.

3.3 Determination of Bjorken Sum Rule

3.3.1 Bjorken sum rule from QCD analysis

The Bjorken sum rule is a fundamental result in pQCD. In this section we present a method of testing this in a way consistent with the pQCD analysis presented so far. The conventional method of testing the Bjorken sum rule (which has been used in most experimental papers) is to evaluate the difference between the first moments of the proton and neutron polarized structure functions at a fixed Q_0^2 and to see if the relation

$$\Gamma_1^{\rm p} - \Gamma_1^{\rm n} = \frac{1}{6}\left|\frac{g_A}{g_V}\right| \cdot C_1^{\rm NS}(Q^2) \tag{16}$$

holds. Here g_A/g_V is the axial vector coupling constant. The coefficient $C_1^{\rm NS}(Q^2)$ has been calculated to $4^{\rm th}$ order in $\alpha_s(Q^2)$ [35].

Based on the pQCD analysis we have evaluated the first moments of the proton and neutron structure functions at $Q_0^2 = 5$ GeV^2 given in Table 7. However, we can not directly use them to evaluate the Bjorken sum rule because in this analysis we have taken the first moments to be: $\eta_{\rm NS}^{\rm p/n} = \pm\frac{3}{4}\left|\frac{g_A}{g_V}\right| + \frac{1}{4}a_8$, with the value of g_A/g_V fixed to its nominal value of 1.2601 ± 0.0025 [28]. In this way the Bjorken sum rule is assumed in the analysis. We can test the validity of the Bjorken sum rule by releasing this constraint in our pQCD analysis and making g_A/g_V one of the free parameters to be fitted by the g_1 data. The best fit parameters for such a fit are given in Table 8. The experimental and theoretical uncertainty study presented in Section 2.7 was repeated for the uncertainty estimation for g_A/g_V. We obtain:

$$\left|\frac{g_A}{g_V}\right| = 1.15\ ^{+0.03}_{-0.03}\ (\text{sta})\ \ ^{+0.07}_{-0.06}\ (\text{sys})\ \ ^{+0.14}_{-0.04}\ (\text{th}). \tag{17}$$

The value of g_A/g_V determined here is consistent with the nominal value used above. The uncertainties (particularly theoretical) are large. The largest contribution to the theoretical uncertainty is the factorization and renormalization scales and due to the choice of the initial parton distributions.

The above value of g_A/g_V and its uncertainty when used to evaluate the value of Bjorken sum in Eq. 16 to order $\mathcal{O}(\alpha_s^2)$ (consistent with all other analysis presented in this paper) at $Q_0^2 = 5$ GeV^2 gives:

$$\begin{aligned} \Gamma_1^{\rm p} - \Gamma_1^{\rm n} &= 0.174 \ {}^{+0.005}_{-0.005}\,(\text{sta}) \ {}^{+0.011}_{-0.009}\,(\text{sys}) \ {}^{+0.021}_{-0.006}\,(\text{th}) \\ &= 0.174 \ {}^{+0.024}_{-0.012} \ , \end{aligned} \tag{18}$$

which is in excellent agreement with the theoretically calculated value of $\Gamma_1^{\rm p} - \Gamma_1^{\rm n} = 0.181 \pm 0.003$ [35] at the same Q_0^2.

3.3.2 QCD evolution of $g_1^{\rm NS}$

An alternative way to determine the Bjorken sum rule is by restricting the QCD analysis to the purely non-singlet combination of the polarized parton distribution functions $\Delta q_{\rm NS}$. It is related to the structure functions, using Eq. 4,

$$g_1^{\rm p}(x,Q^2) - g_1^{\rm n}(x,Q^2) = \frac{1}{2}\langle e^2\rangle \int_x^1 \frac{{\rm d}y}{y}\left[C_{1,\rm NS}(\tfrac{x}{y},\alpha_s(t))\,\Delta q_{\rm NS}(y,t)\right], \tag{19}$$

where $t = \ln(Q^2/\Lambda^2)$. The Q^2 dependence of $\Delta q_{\rm NS}$ is described by the DGLAP evolution equation for the non-singlet combination (Eq.8) and is decoupled from the evolution of $\Delta\Sigma$ and Δg. Thus, having $g_1^{\rm p} - g_1^{\rm n}$ data points at different values of Q^2 allows us to determine g_A/g_V by parametrizing only $\Delta q_{\rm NS}$ at an initial scale Q_i^2, evolving it, and fitting the parameters including g_A/g_V to the data. The advantage of this method is that the analysis can be performed with fewer free parameters than the standard analysis presented in the previous sections. We use the parametrization:

$$\Delta q_{\rm NS}(x,Q^2) = \frac{3}{2}\left|\frac{g_A}{g_V}\right| \cdot N(\alpha,\beta)\cdot x^{\alpha}(1-x)^{\beta}, \tag{20}$$

with α, β, and g_A/g_V being the three free parameters of the fit. However, there is a disadvantage to this method. In order to evaluate the value of $g_1^{\rm p} - g_1^{\rm n}$ to be used in this fit, the values of the proton and neutron structure functions should be known ideally the same values of x and Q^2. This is true only for SMC [1] and E143 [18, 19, 20] data. The SMC data points for $g_1^{\rm p}$ and $g_1^{\rm d}$ were combined as explained in Ref. [1]. The E143 data were treated similarly. In all we obtain 44 data points for $g_1^{\rm NS}$ (12 from SMC and 32 from E143). The general procedure of the analysis is the same as explained in Section 2.3 except that here it is done only with the nonsinglet parton distribution. The initial scale $Q_i^2 = 1$ GeV^2 was used in this analysis as it was in the global pQCD analysis.

The values of the fitted parameters are given in Table 9. The result of the fit at $Q_0^2 = 5$ GeV^2 is displayed in Fig. 10. The data points evolved to the same $Q_0^2 = 5$ GeV^2 are shown with their statistical errors. The bold line is the curve calculated using the best fit parameters. The area under this line corresponds to the Bjorken integral $\Gamma_1^{\rm NS-fit}$. The uncertainty band around this line shows the total uncertainty estimated from the experimental systematic and theoretical sources. The uncertainty (experimental

systematic and that of theoretical origin) for the fitted value of g_A/g_V was estimated. We get:

$$\left|\frac{g_A}{g_V}\right| = 1.20\ ^{+0.08}_{-0.07}\ (\text{sta})\ ^{+0.12}_{-0.12}\ (\text{sys})\ ^{+0.10}_{-0.04}\ (\text{th}).$$

At $Q_0^2 = 5$ GeV^2 this value of g_A/g_V corresponds to the Bjorken sum:

$$\begin{aligned}\Gamma_1^{\mathrm{p}} - \Gamma_1^{\mathrm{n}} &= 0.181\ ^{+0.012}_{-0.011}\ (\text{sta})\ ^{+0.018}_{-0.018}\ (\text{sys})\ ^{+0.015}_{-0.006}\ (\text{th}) \\ &= 0.181\ ^{+0.026}_{-0.021} \end{aligned} \quad (21)$$

using Eq. 16 when evaluated at $\mathcal{O}(\alpha_s^2)$. The result for g_A/g_V agrees well with the nominal value and with the results of the standard fit with g_A/g_V as a free parameter (Eq. 17). Because of the smaller data set used the errors of experimental origin are significantly larger. However note that the theoretical error is slightly lower than in the case of the standard fit.

The contribution to the Bjorken sum from the measured x region calculated from the data points and by integrating the fitted function are given in Table 10 in columns 4 and 5, respectively. They are given for combined SMC+E143 data at $Q_0^2 = 5$ GeV^2 as well as for SMC data at $Q_0^2 = 10$ GeV^2. In both cases the integral over the measured x range evaluated using the data and that evaluated using the best fit parameters agree within the statistical precision of the data. The high x contribution to the integral makes little impact on the nonsinglet first moment. At both values of Q_0^2 the contributions to the integrals Γ_1^{NS} from the unmeasured low x region are $\approx 5\%$ of the total integral with small uncertainties. Hence we note that although the uncertainties in the first moments of the proton and neutron are large (Tables V and VII), the uncertainty in the Bjorken integral from this region is rather small.

3.3.3 Comments on Bjorken sum rule determination

In Section 3.3.1 we have presented a determination of the Bjorken sum rule, based on the final SMC data set and all other published data on g_1. The result was obtained in a NLO QCD analysis by directly fitting the value of g_A/g_V. This is our best determination of the Bjorken sum in a fully consistent way based on pQCD using the world data set.

The result we obtain is consistent with the expected value and we confirm the Bjorken sum rule with an accuracy of $\approx 10\%$. It also agrees well with the results of the NLO QCD analysis of the E154 collaboration [9]. Our estimate of the uncertainty is larger for the following reason: we have taken the view that the errors due to the factorization and renormalization scales and those due to α_s are uncorrelated where as they have treated them as correlated. If we follow their approach, the uncertainties become comparable.

The method used in Section 3.3.2 to test the Bjorken sum rule from g_1^{NS} is potentially very precise with regard to the theoretical uncertainty. It leads to a confirmation of the Bjorken sum rule at the level of $\approx 15\%$. At present this method suffers from a limited statistical accuracy but it is expected to be more powerful once the very precise data on g_1^{p} from E155 [36] become available and are combined with the existing data on g_1^{n} from E154 [22].

4 Conclusions and Summary

We have performed a next-to-leading order pQCD analysis of the world data on polarized deep inelastic inclusive scattering, including new data from SMC. The results of the pQCD fit are used to evaluate contributions to the first moment of g_1 over the

entire x range. Consistent values of the singlet axial charge a_0 are obtained from the first moments and from the fit parameters.

The experimental data constrain the quark singlet and non-singlet distributions rather well. This was tested using two different analysis programs. The polarized structure functions are equally well reproduced by fits in the $\overline{\rm MS}$ and the AB factorization schemes, although the shapes of the singlet distributions are found to be different. The singlet and nonsinglet quark distributions are well determined, while the gluon distribution is only poorly constrained by the fits. The gluon first moment is found to be positive but has an error of the order of 100 % of its value. The singlet axial charge is found to be $\approx 1/3$ of the value expected from the naive QPM.

Inclusion of the strong coupling constant α_s as a free parameter in the fit results in a value for α_s in excellent agreement with the one obtained from the observation of scaling violations in unpolarized DIS data. However, this determination based on g_1 also involves F_2 and hence is not independent of the determination of α_s from F_2.

The Bjorken sum rule has been tested in two different ways: in a global pQCD analysis and in an analysis restricted to the non-singlet part of g_1 performed using a subset of the available data. In both cases $|g_A/g_V|$ was left as a free parameter of the fit. The sum rule is found to be verified in both cases, within an accuracy of about 10% for the global fit and 15% for the non-singlet fit.

In the near future, the additional high precision data from SLAC E155 are expected to improve the accuracy of the QCD fit. However due to the absence of data in the low x region, contribution to the first moment from this region is expected to be the largest source of uncertainty. Improved determinations of the polarized gluon distribution will be obtained by dedicated experiments e.g. COMPASS [37] at CERN and PHENIX and STAR experiments at the RHIC-Spin [38]. Measurements of the spin structure function in the presently inaccessible low x region using the HERA polarized collider [39] will provide crucial information on the low x behavior of g_1 and also allow access to the polarized gluon distribution in that region.

ACKNOWLEDGMENT

We thank G. Altarelli, R. D. Ball, S. Forte, T. Gehrmann, G. Ridolfi, and W. Vogelsang for many interesting discussions. Special thanks are due to R. D. Ball, S. Forte and G. Ridolfi for providing us with the pQCD analysis code.

This work was supported by Bundesministerium für Bildung, Wissenschaft, Forschung und Technologie, partially supported by TUBITAK and the Center for Turkish-Balkan Physics Research and Application (Bogziçi University), supported by the U.S. Department of Energy, the U.S. National Science Foundation, Monbusho Grant-in-Aid for Science Research (International Scientific Research Program and Specially Promoted Research), the National Science Foundation (NWO) of the Netherlands, the Commisariat à l'Energie Atomique, Comision Interministerial de Ciencia y Tecnologia and Xunta de Galicia, the Israel Science Foundation, and Polish State Committee for Scientific Research (KBN) Grant No. 2/P03B/081/14.

References

[1] SMC, *Spin Asymmetries A_1 and Structure Functions g_1 of the Proton and Deuteron from Polarized High Energy Muon Scattering*, Submitted to Phys. Rev. **D** with this paper.

[2] J. Ellis and R.L. Jaffe, Phys. Rev. D **9**, 1444 (1974); *ibid.* D **10**, 1669 (1974).

[3] G. Altarelli and G.G. Ross, Phys. Lett. B **212**, 391 (1988); A. V. Efremov and O. V. Teryaev, JINR Report No. E2-88-287, Dubna, (1988); R. D. Carlitz, J. C. Collins, and A. H. Mueller, Phys. Lett. B **214**, 229 (1988).
[4] J.D. Bjorken, Phys. Rev. **148**, 1467 (1966); *ibid.* D **1**, 1376 (1970).
[5] M.Glück, E. Reya, M. Stratmann and W. Vogelsang, Phys. Rev. D **53**, 4775 (1996).
[6] R.D. Ball, S. Forte and G. Ridolfi, Phys. Lett. B **378**, 255 (1996).
[7] T. Gehrmann and W.J. Stirling, Z. Phys. C **65**, 461 (1995); Phys. Rev. D **53**, 6100 (1996).
[8] G. Altarelli, R.D. Ball,S. Forte and G. Ridolfi, Nucl. Phys. B **496** 337 (1997).
[9] E154, K. Abe *et al.*, Phys. Lett. B **405**, 180 (1997).
[10] SMC, D. Adams *et al.*, Phys. Lett. B **396**, 338 (1997).
[11] SMC, B. Adeva *et al.*, Phys. Lett. B **412**, 414 (1997).
[12] SMC, D. Adams *et al.*, Phys. Rev. D **56**, 5330 (1997).
[13] NMC, M. Arneodo *et al.*, Nucl. Phys. B **483**, 3 (1997).
[14] L. W. Whitlow *et al.*, Nucl. Phys. **282**, 475 (1992).
[15] H.-Y. Cheng, Chin. J. Phys. **35**, 25 (1996).
[16] V.W. Hughes and J. Kuti, Ann. Rev. Nucl. Part. Sci. **33**, 611 (1983); T. Pussieux and R. Windmolders, in: *Internal Spin Structure of the Nucleon*, ed. by V.W. Hughes and C. Cavata (World Scientific, Singapore, 1995), p. 212.
[17] EMC, J. Ashman *et al.*, Phys. Lett. B **206**, 364 (1988); Nucl. Phys. B **328**, 1 (1989).
[18] E143, K. Abe *et al.*, Phys. Rev. Lett. **74**, 346 (1995).
[19] E143, K. Abe *et al.*, Phys. Rev. Lett. **75**, 25 (1995).
[20] E143, K. Abe *et al.*, Phys. Lett. B **364**, 61 (1995).
[21] E142, P. Anthony *et al.*, Phys. Rev. D **54**, 6620 (1996).
[22] E154, K. Abe *et al.*, Phys. Rev. Lett. **79**, 26 (1997).
[23] HERMES, K. Ackerstaff *et al.*, Phys. Lett. B **404**, 383 (1997).
[24] V.N. Gribov and L.N. Lipatov, Sov. Journ. Nucl. Phys. **15**, 438 (1972); **15**, 675 (1972); G. Altarelli and G. Parisi, Nucl. Phys. B **126**, 298 (1977); Yu. L. Dokshitzer, Sov. Phys. JETP **46**, 641 (1977).
[25] J. Kodaira *et al.*, Phys. Rev. D **20**, 627 (1979); J. Kodaira, Nucl. Phys. B **165**, 129 (1980).
[26] R. Mertig and W.L. van Neerven, Z. Phys. C **70**, 637 (1996); W. Vogelsang, Nucl. Phys. B **475**, 47 (1996).
[27] R. G. Roberts, *The structure of the proton*, Cambridge Monographs on Mathematical Physics (1990).
[28] Particle Data Group, R.M. Barnett *et al.*, Phys. Rev. D **54**, 1 (1996).
[29] F.E. Close and R.G. Roberts, Phys. Lett. B **316**, 165 (1993).
[30] S. J. Brodsky, M. Burkardt, and I. Schmidt, Nucl. Phys. B **441**, 197 (1995).
[31] D. Fasching, Ph.D thesis, Northwestern University (1996), and `hep-ph/9610261` (unpublished).
[32] NMC, M. Arneodo *et al.*, Phys. Lett. B **309**, 222 (1993); M. Virchaux and A. Milsztajn, Phys. Lett. B **274**, 221 (1992); CCFR Collaboration, W.G. Seligman *et al.*, Phys. Rev. Lett. **79**, 1213 (1997); R.D. Ball and S. Forte in *Proceedings of DIS96, Rome, April 1996.*
[33] J. Saborido, Ph.D. Thesis, University of Santiago de Compostela (1995).
[34] E. P. Sichtermann, Ph.D. Thesis, Free University of Amsterdam (1998).
[35] S.A. Larin, F.V. Tkachev and J.A.M. Vermaseren, Phys. Rev. Lett. **66**, 862 (1991); S.A. Larin and J.A.M. Vermaseren, Phys. Lett. B **259** 345 (1991).

[36] E155, e.g. C. Young in *Proc. of the Workshop: 'Deep Inelastic Scattering off Polarized Targets'*, ed. by J. Blümlein *et al.*, DESY 97-200, 12 (1997).
[37] COMPASS proposal, CERN/SPSLC/P297, March 1996.
[38] Y. I. Makdisi, *Proc. of '12th Int. Symposium on High Energy Spin Physics'*, Amsterdam 1996, ed. by C.W. de Jager *et al.*, (World Scientific, Singapore, 1997), p107.
[39] A. Deshpande *et al.*, *Proceedings of the workshop: 'Physics with Polarized Protons at HERA'*, edited by A. De Roeck and T. Gehrmann, DESY-Proceedings-1998-01, p. 26; G. Rädel *et al.*, DESY-Proceedings-1998-01, p. 54; A. de Roeck *et al.*, `hep-ph/9801300` to be published in European Physical Journal **C**.

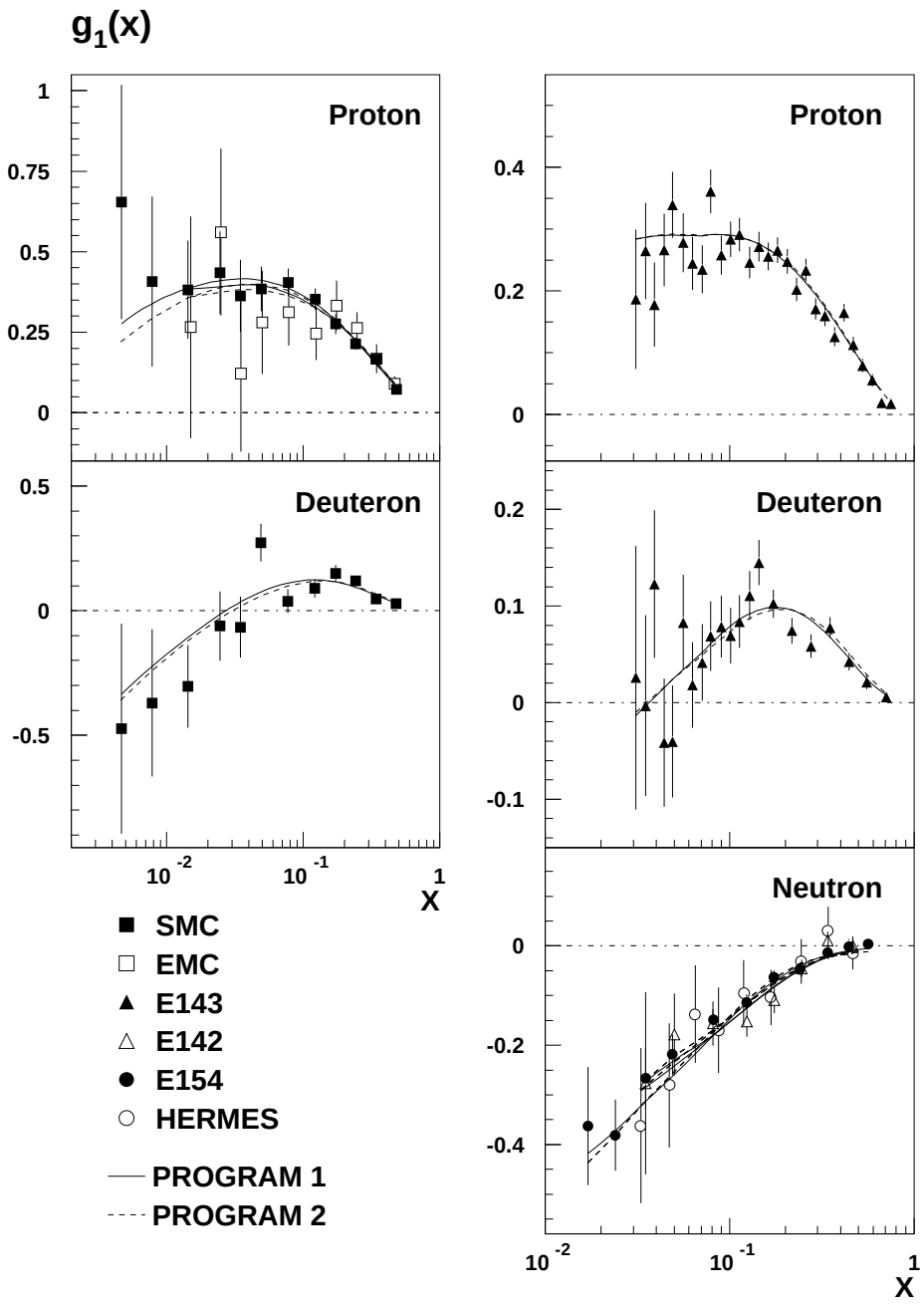

Figure 1: Comparison of the two programs in the $\overline{\rm MS}$ Scheme. Data on $g_1^{\rm p,d,n}$ from CERN experiments (left column), SLAC and DESY experiments (right column) are shown at their measured Q^2 with their statistical errors. The results of the QCD fits using the two programs at the measured Q^2 of the data are shown by continuous and dashed lines in each plot. Note that some of the fits for SLAC and DESY experiments (right column) are almost indistinguishable.

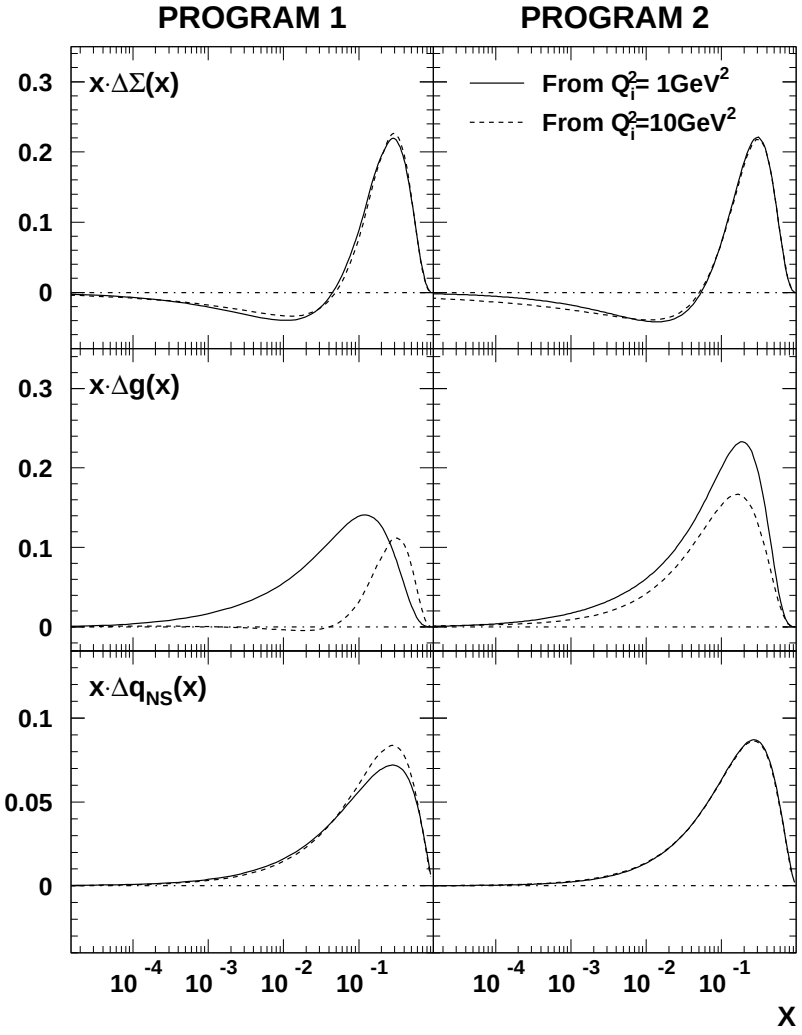

Figure 2: Polarized parton distribution functions at $Q_0^2 = 5$ GeV^2 resulting from the fits using Program 1 (left) and Program 2 (right) with initial scales of $Q_i^2 = 1$ GeV^2 and 10 GeV^2.

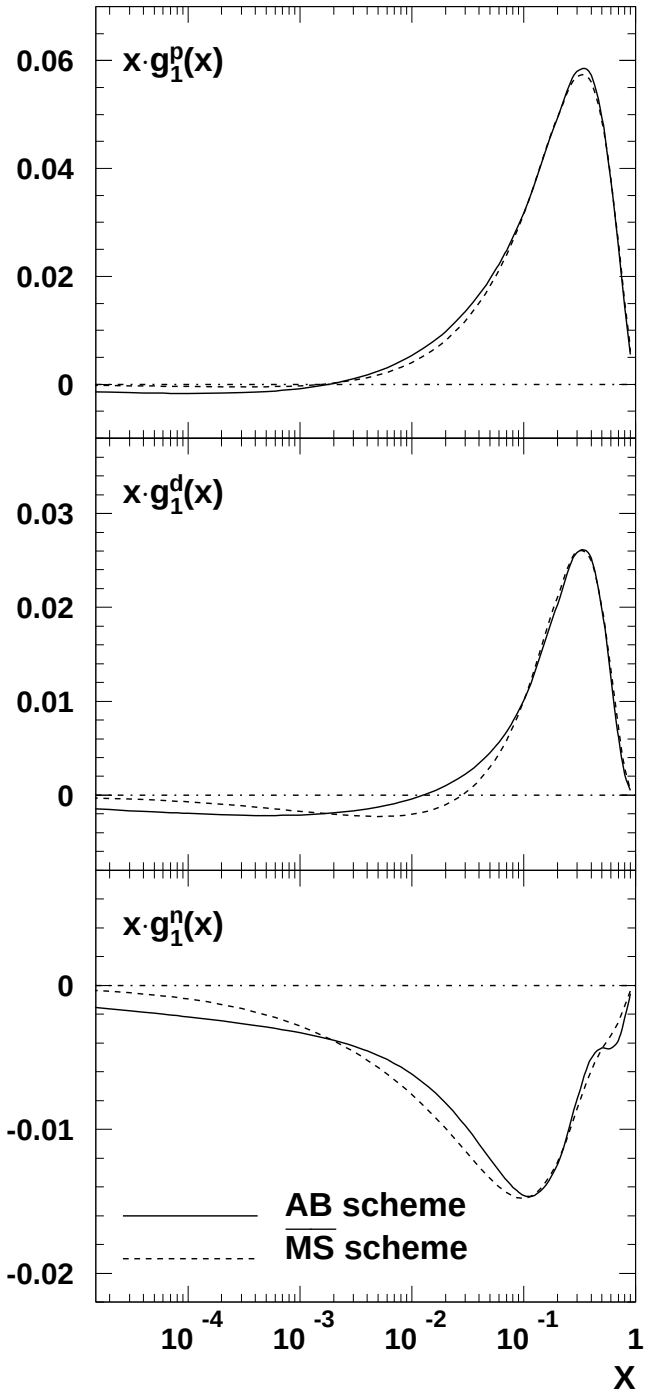

Figure 3: $xg_1^{\mathrm{p,d,n}}$ vs. x: Comparison of fits done in two different schemes: $\overline{\mathrm{MS}}$ and AB. All distributions are given at $Q^2 = 5$ GeV^2. The wiggle in xg_1^{n} is in a region of x which has little data. The uncertainty in the QCD fit in this region is large (see Fig. 8), consequently, the wiggle itself has no physical significance.

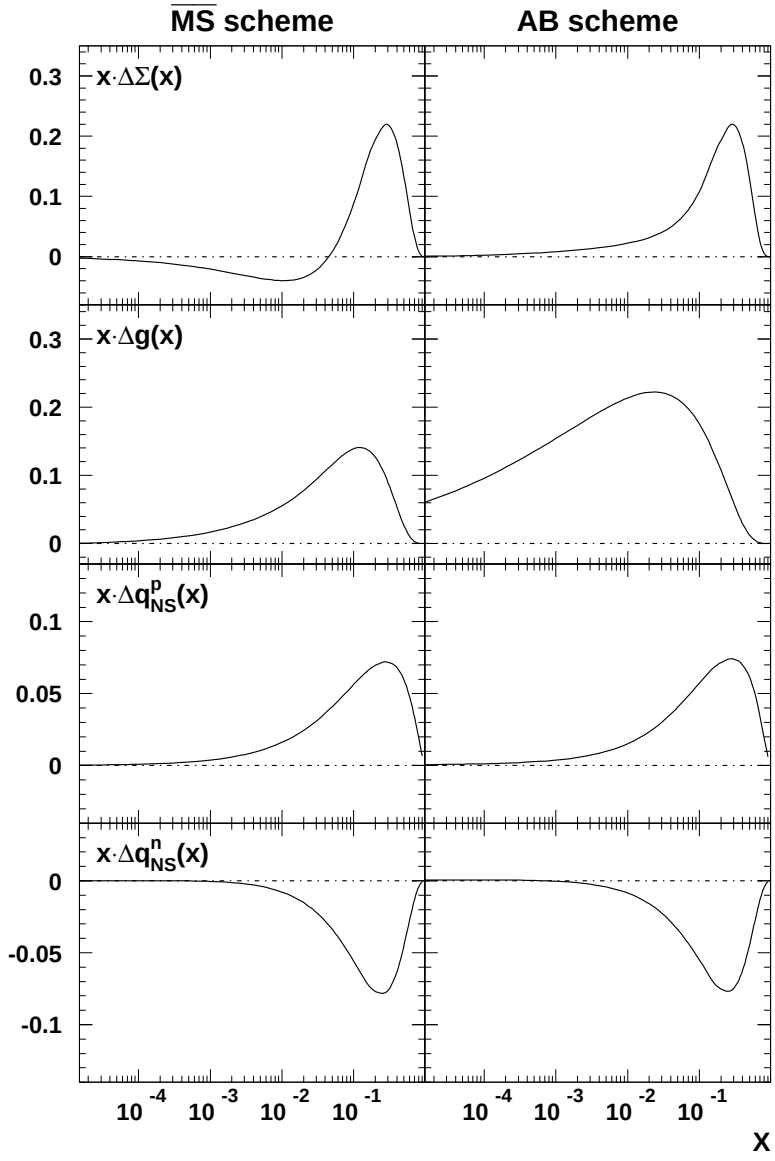

Figure 4: Polarized parton distribution functions at $Q_0^2 = 5\ \mathrm{GeV}^2$ obtained in two different schemes: $\overline{\mathrm{MS}}$ and AB.

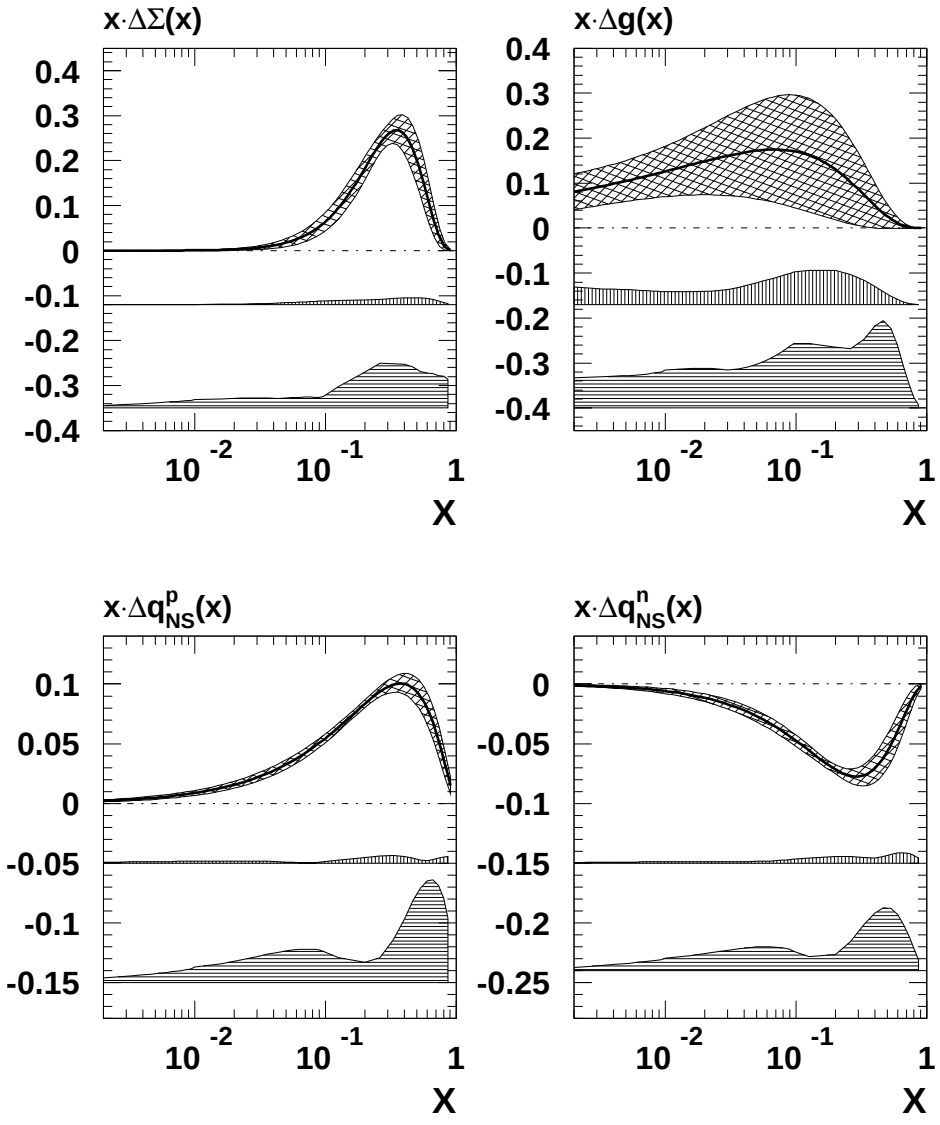

Figure 5: Polarized parton distribution functions determined from the pQCD analysis at $Q_i^2 = 1$ GeV^2. Their statistical uncertainty as obtained from the QCD fit is shown by a band with crossed hatch. The experimental systematic uncertainty is indicated by the vertically hatched band, and the theoretical uncertainty by the horizontally hatched band.

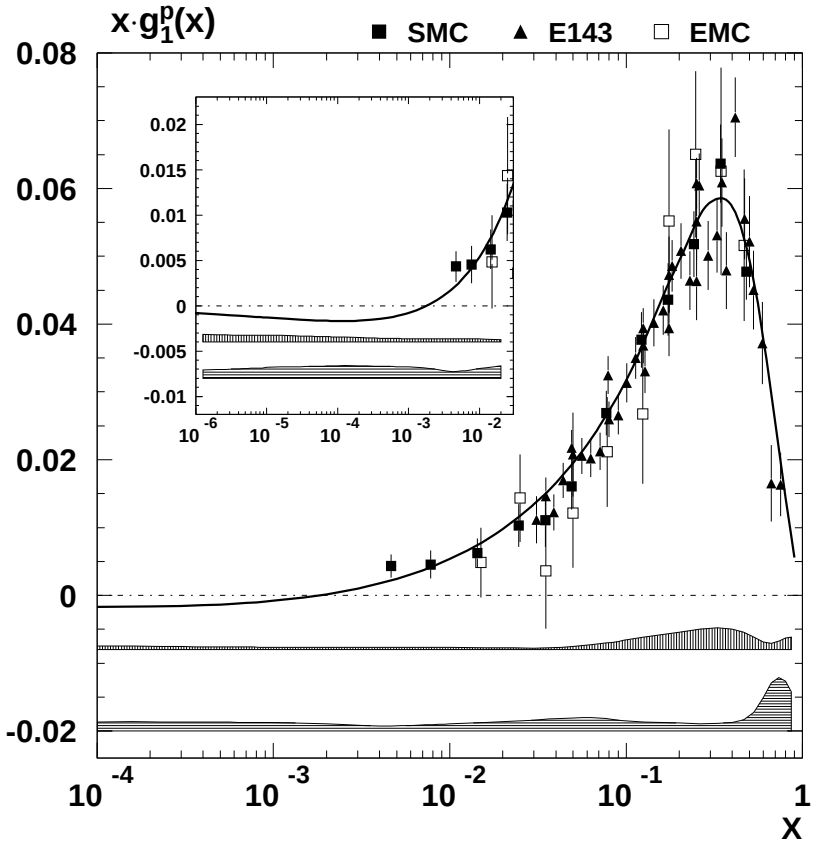

Figure 6: xg_1^{p} vs. x for the world data with the QCD fit at $Q^2 = 5$ GeV^2. The low x region is emphasized in the inset. The data points are shown with their statistical errors. The uncertainties of the fit due to experimental systematics and theoretical sources are shown by the vertically and horizontally hatched bands, respectively.

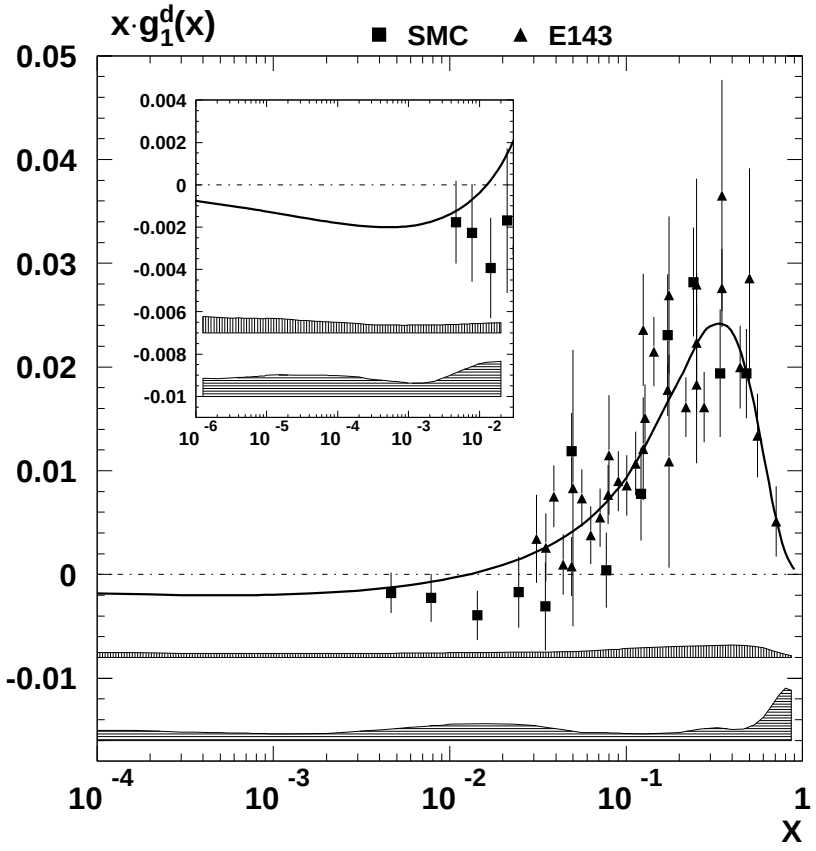

Figure 7: $xg_1^{\rm d}$ vs. x for the world data with the QCD fit at $Q^2 = 5$ GeV^2. The low x region is emphasized in the inset. The data points are shown with their statistical errors. The uncertainties of the fit due to experimental systematics and theoretical sources are shown by the vertically and horizontally hatched bands, respectively.

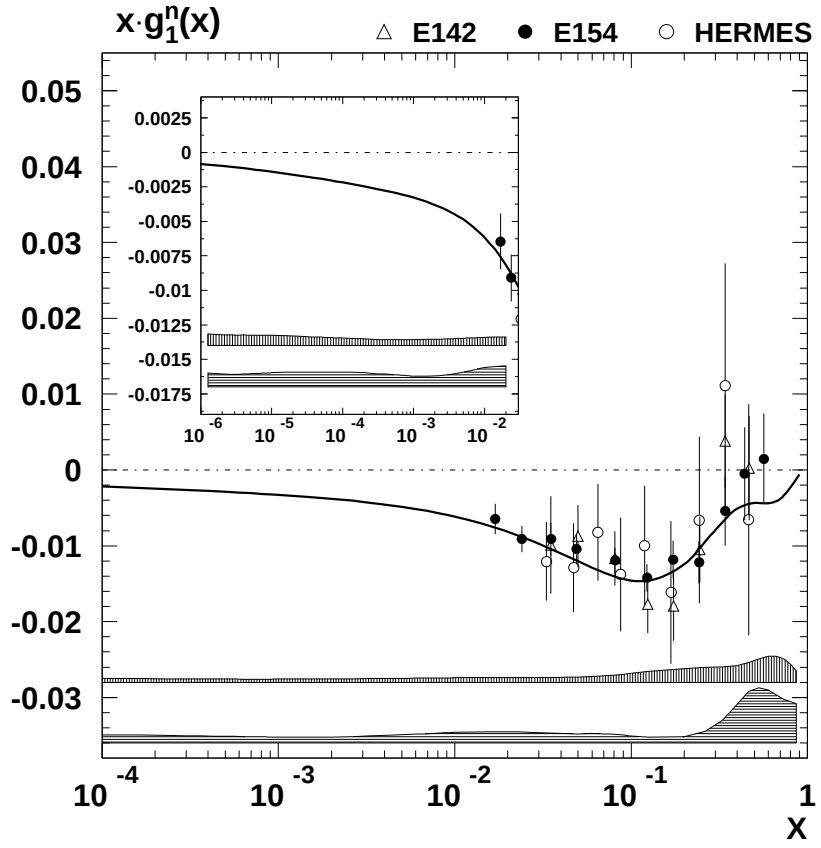

Figure 8: xg_1^{n} vs. x for the world data with the QCD fit at $Q^2 = 5$ GeV^2. Only statistical errors are shown with the data points. The low x region is emphasized in the inset. The uncertainties in the fit due to experimental systematics and theoretical sources are shown by the vertically and horizontally hatched bands, respectively.

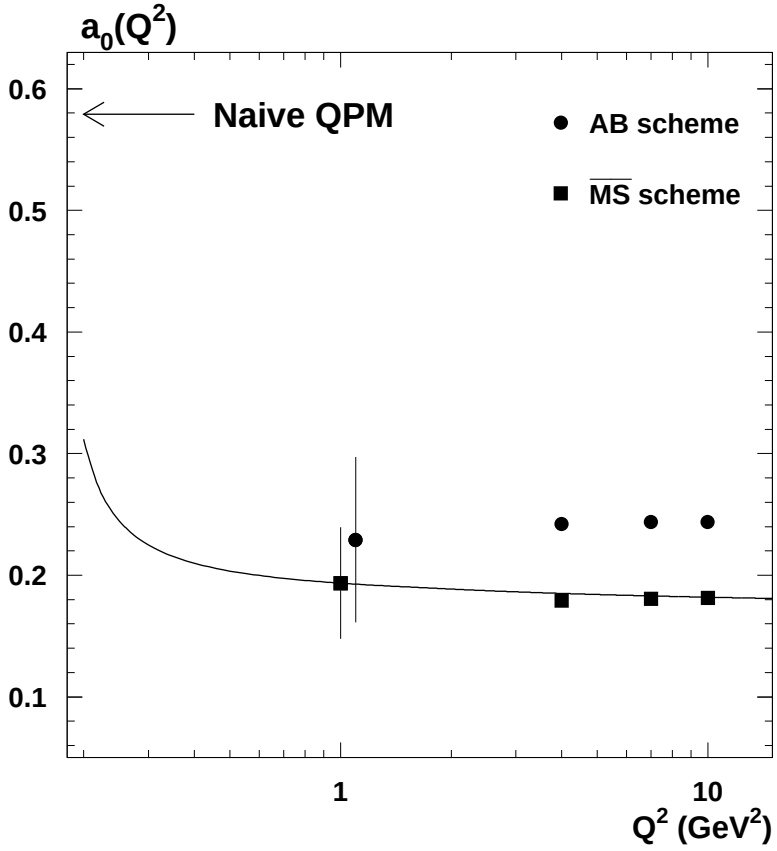

Figure 9: The Q^2 dependence of a_0 determined in this analysis using different schemes and with different starting scales Q_i^2 is shown. The curve shows the predicted Q^2 evolution of a_0 in the $\overline{\text{MS}}$ scheme. The statistical errors in a_0 are shown only for $Q_i^2 = 1$ GeV^2. The uncertainties for the other points at higher Q_i^2 values are comparable. The expectation for the value of a_0 based on the naive QPM is also shown for comparison.

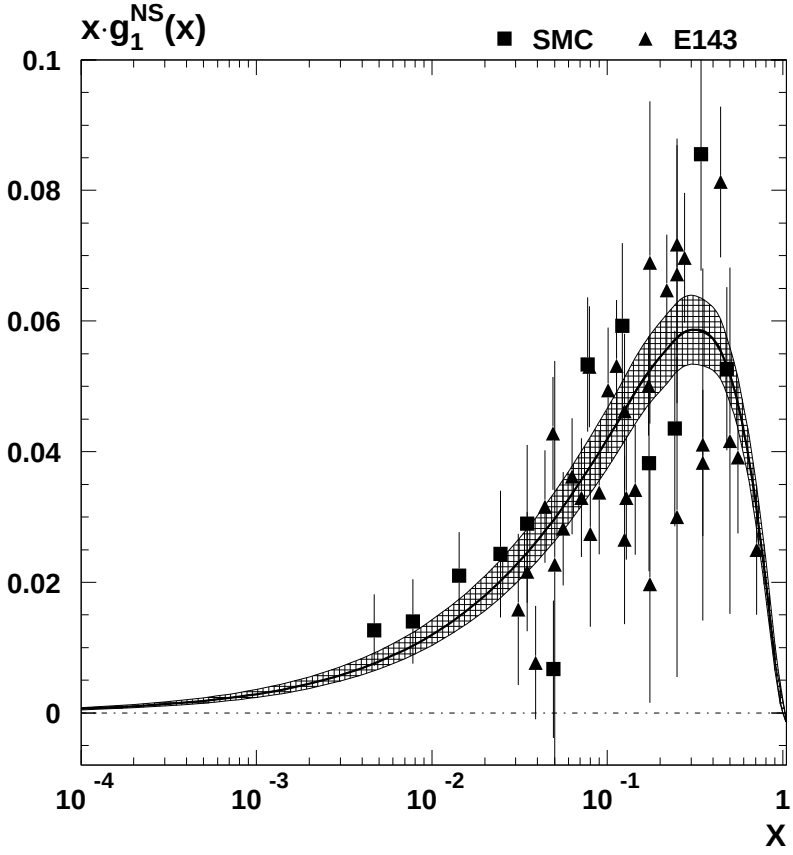

Figure 10: The result of the best fit to xg_1^{NS} together with the data points used in the fit evolved to $Q^2 = 5$ GeV^2. The error bars on the data points show statistical errors only, while the error band around the curve (cross hatch) represents the systematic uncertainty of the fit, including contributions from experimental systematic and theoretical sources.

Table 1: Comparison of results for the fitted parameters obtained with the two programs. The results are given for fits with an initial scale $Q_i^2 = 1$ GeV^2 and $Q_i^2 = 10$ GeV^2. All fits are performed in the $\overline{\rm MS}$ scheme. The uncertainties are statistical only.

	$Q_i^2 = 1$ GeV^2		$Q_i^2 = 10$ GeV^2	
Parameter	Program 1	Program 2	Program 1	Program 2
$\eta_{\rm S}$	$0.19^{+0.04}_{-0.05}$	$0.18^{+0.04}_{-0.05}$	$0.18^{+0.04}_{-0.07}$	$0.12^{+0.08}_{-0.17}$
$\alpha_{\rm S}$	$-0.46^{+0.12}_{-0.11}$	$-0.43^{+0.13}_{-0.13}$	$-0.61^{+0.12}_{-0.13}$	$-0.72^{+0.10}_{-0.16}$
$\beta_{\rm S}$	$3.05^{+0.38}_{-0.35}$	$3.23^{+0.41}_{-0.38}$	$3.81^{+0.43}_{-0.42}$	$3.60^{+0.63}_{-0.43}$
$a_{\rm S}$	$-13.0^{+1.2}_{-1.4}$	$-12.2^{+1.3}_{-1.5}$	$-21.0^{+2.9}_{-4.0}$	$-22.9^{+5.2}_{-6.8}$
η_g	$0.21^{+0.27}_{-0.21}$	$0.38^{+0.29}_{-0.28}$	$0.22^{+0.19}_{-0.18}$	$0.61^{+1.80}_{-0.55}$
α_g	$0.48^{+3.24}_{-1.36}$	$1.02^{+1.44}_{-1.25}$	$0.56^{+0.75}_{-0.94}$	$-0.44^{+1.30}_{-0.48}$
$\alpha_{\rm NS}$	$-0.11^{+0.05}_{-0.05}$	$-0.12^{+0.05}_{-0.05}$	$-0.29^{+0.03}_{-0.03}$	$-0.29^{+0.03}_{-0.03}$
$\beta_{\rm NS}$	$1.69^{+0.16}_{-0.16}$	$1.68^{+0.15}_{-0.15}$	$2.22^{+0.16}_{-0.15}$	$2.12^{+0.16}_{-0.15}$
χ^2	127.4	119.8	122.6	118.8
d.f.	$133 - 8$	$133 - 8$	$133 - 8$	$133 - 8$

Table 2: Comparison of results of the QCD fits at $Q^2 = 1$ GeV^2 in the $\overline{\rm MS}$ scheme and the AB scheme. The errors are statistical only.

Parameter	$\overline{\rm MS}$	AB
$\eta_{\rm S}$	$0.19^{+0.04}_{-0.05}$	$0.38^{+0.03}_{-0.03}$
$\alpha_{\rm S}$	$-0.48^{+0.11}_{-0.10}$	$1.20^{+0.29}_{-0.27}$
$\beta_{\rm S}$	$3.29^{+0.40}_{-0.37}$	$4.08^{+0.63}_{-0.58}$
$a_{\rm S}$	$-13.8^{+1.3}_{-1.5}$	(0.0)
η_g	$0.25^{+0.29}_{-0.22}$	$0.99^{+1.17}_{-0.31}$
α_g	$0.33^{+2.05}_{-1.05}$	$-0.70^{+0.23}_{-0.20}$
$\alpha^{\rm p}_{\rm NS}$	$-0.19^{+0.09}_{-0.08}$	$-0.15^{+0.09}_{-0.08}$
$\beta^{\rm p}_{\rm NS}$	$1.35^{+0.23}_{-0.21}$	$1.42^{+0.23}_{-0.22}$
$\alpha^{\rm n}_{\rm NS}$	$0.06^{+0.14}_{-0.13}$	$0.01^{+0.13}_{-0.12}$
$\beta^{\rm n}_{\rm NS}$	$2.59^{+0.52}_{-0.48}$	$2.48^{+0.51}_{-0.46}$
χ^2	122.9	126.3
d.f.	$133-10$	$133-9$

Table 3: The best fit parameters of the pQCD fit when $\alpha_s(M_Z^2)$ was made a free parameter. All parameters are given at $Q^2 = 1$ GeV^2 except for the value of α_s which is given at $Q^2 = M_Z^2$ GeV^2. The uncertainties are statistical only.

Parameter	Value	Parameter	Value
$\eta_{\rm S}$	$0.39^{+0.03}_{-0.03}$	η_g	$0.98^{+7.41}_{-0.37}$
$\alpha_{\rm S}$	$1.22^{+0.28}_{-0.27}$	α_g	$-0.78^{+0.22}_{-0.21}$
$\beta_{\rm S}$	$4.00^{+0.63}_{-0.60}$	β_g	(4.0)
$\eta^{\rm p}_{\rm NS}$	$\frac{3}{4}\lvert\frac{g_A}{g_V}\rvert + \frac{1}{4}a_8$	$\eta^{\rm n}_{\rm NS}$	$-\frac{3}{4}\lvert\frac{g_A}{g_V}\rvert + \frac{1}{4}a_8$
$\alpha^{\rm p}_{\rm NS}$	$-0.08^{+0.11}_{-0.10}$	$\alpha^{\rm n}_{\rm NS}$	$0.04^{+0.14}_{-0.13}$
$\beta^{\rm p}_{\rm NS}$	$1.53^{+0.26}_{-0.24}$	$\beta^{\rm n}_{\rm NS}$	$2.60^{+0.54}_{-0.49}$
$\alpha_s(M_Z^2)$	$0.121^{+0.002}_{-0.002}$		
χ^2	125.1		
d.f.	$133-10$		

Table 4: First moments of the nucleon spin structure functions at $Q_0^2 = 5$ GeV^2 in the measured x range from 0.003 to 0.8. The first uncertainty is statistical, the second experimental systematic, and the third due to the uncertainty in evolution. For comparison, the integral over the QCD fit is given in the third column.

Nucleon	$\int_{0.003}^{0.8} g_1(x, Q_0^2)\mathrm{d}x$	$\int_{0.003}^{0.8} g_1^{\mathrm{fit}}(x, Q_0^2)\mathrm{d}x$
Proton	$0.130 \pm 0.003 \pm 0.005 \pm 0.004$	0.132
Deuteron	$0.036 \pm 0.004 \pm 0.003 \pm 0.002$	0.040
Neutron	$-0.054 \pm 0.007 \pm 0.005 \pm 0.004$	-0.048

Table 5: First moments of the structure functions at $Q_0^2 = 5$ GeV^2 from the unmeasured x regions and their total uncertainties due to the experimental systematics and the theoretical sources in the evolution.

$\int g_1^{\mathrm{fit}}(x, Q_0^2)\mathrm{d}x$	$0.0 < x < 0.003$	$0.8 < x < 1.0$
Proton	$-0.012^{+0.014}_{-0.025}$	$0.003^{+0.001}_{-0.001}$
Deuteron	$-0.015^{+0.010}_{-0.023}$	$0.000^{+0.000}_{-0.001}$
Neutron	$-0.020^{+0.010}_{-0.026}$	$0.000^{+0.001}_{-0.001}$

Table 6: Uncertainties on the first moments resulting from the pQCD analysis separated by sources given in this table in three parts. In the top part the first moments of $g_1^{p,d,n}$ at $Q_0^2 = 5$ GeV^2 are given with their total experimental systematic and theoretical uncertainties. In the central part the total experimental systematic uncertainty from above is split into contributions from different experiments, while in the lowest part the total theoretical uncertainty is split into its sources.

Nucleon	Γ_1^{fit}	Total Exp. Sys.	Total Theory	
Proton	0.122	$^{+0.007}_{-0.011}$	$^{+0.007}_{-0.024}$	
Deuteron	0.025	$^{+0.006}_{-0.010}$	$^{+0.006}_{-0.020}$	
Neutron	-0.068	$^{+0.007}_{-0.011}$	$^{+0.005}_{-0.020}$	
Exp. Sys.	**SMC**	**E154**	**E143**	**Other Exp.**
Proton	$^{+0.005}_{-0.008}$	$^{+0.005}_{-0.005}$	$^{+0.000}_{-0.004}$	$^{+0.001}_{-0.002}$
Deuteron	$^{+0.004}_{-0.008}$	$^{+0.005}_{-0.005}$	$^{+0.000}_{-0.003}$	$^{+0.001}_{-0.002}$
Neutron	$^{+0.005}_{-0.008}$	$^{+0.005}_{-0.005}$	$^{+0.000}_{-0.004}$	$^{+0.001}_{-0.002}$
Theory	**Scale**	**α_s**	**PDF**	**Others**
Proton	$^{+0.005}_{-0.024}$	$^{+0.002}_{-0.004}$	$^{+0.004}_{-0.001}$	$^{+0.002}_{-0.002}$
Deuteron	$^{+0.003}_{-0.020}$	$^{+0.001}_{-0.003}$	$^{+0.004}_{-0.001}$	$^{+0.001}_{-0.001}$
Neutron	$^{+0.002}_{-0.020}$	$^{+0.001}_{-0.003}$	$^{+0.005}_{-0.001}$	$^{+0.001}_{-0.001}$

Table 7: Table of $\Gamma_1^{p,d,n}$ at $Q_0^2 = 5$ GeV^2 for the world set of data (left), and at $Q_0^2 = 10$ GeV^2 for SMC (right).

$\Gamma_1(Q_0^2)$	World $Q_0^2 = 5$ GeV^2	SMC $Q_0^2 = 10$ GeV^2
Proton	$0.121 \pm 0.003 \pm 0.005 \pm 0.017$	$0.120 \pm 0.005 \pm 0.006 \pm 0.014$
Deuteron	$0.021 \pm 0.004 \pm 0.003 \pm 0.016$	$0.019 \pm 0.006 \pm 0.003 \pm 0.013$
Neutron	$-0.075 \pm 0.007 \pm 0.005 \pm 0.019$	$-0.078 \pm 0.013 \pm 0.008 \pm 0.014$

Table 8: Best parameters at $Q^2 = 1$ GeV^2 when g_A/g_V is a free parameter in the fit. The uncertainties shown are statistical only.

Parameter	Value	Parameter	Value
η_S	$0.38^{+0.03}_{-0.02}$	η_g	$0.94^{+1.26}_{-0.29}$
α_S	$1.03^{+0.29}_{-0.27}$	α_g	$-0.71^{+0.22}_{-0.21}$
β_S	$3.64^{+0.63}_{-0.59}$	β_g	(4.0)
$\lvert\frac{g_A}{g_V}\rvert$	$1.15^{+0.03}_{-0.03}$		
$\eta^{\rm p}_{\rm NS}$	$\frac{3}{4}\lvert\frac{g_A}{g_V}\rvert + \frac{1}{4}a_8$	$\eta^{\rm n}_{\rm NS}$	$-\frac{3}{4}\lvert\frac{g_A}{g_V}\rvert + \frac{1}{4}a_8$
$\alpha^{\rm p}_{\rm NS}$	$-0.01^{+0.10}_{-0.10}$	$\alpha^{\rm n}_{\rm NS}$	$0.20^{+0.16}_{-0.14}$
$\beta^{\rm p}_{\rm NS}$	$1.86^{+0.30}_{-0.28}$	$\beta^{\rm n}_{\rm NS}$	$3.48^{+0.70}_{-0.63}$
χ^2	116.1		
d.f.	$133 - 10$		

Table 9: Best fit parameters for the $g_1^{\rm NS}$ fit with their statistical errors.

Parameter	Value
$\lvert\frac{g_A}{g_V}\rvert$	$1.20^{+0.08}_{-0.07}$
α	$-0.20^{+0.13}_{-0.12}$
β	$1.42^{+0.40}_{-0.36}$
χ^2	52.4
d.f.	$44 - 3$

Table 10: Integrals of the nonsinglet structure function in the measured and unmeasured x ranges. Integrals are calculated using data (column 4) and using fit parameters (column 5) at $Q^2 = 5$ GeV^2 using the SMC and E143 data, and at $Q_0^2 = 10$ GeV^2 using only SMC data. The indicated uncertainties in the measured x range are the statistical and systematic uncertainties, respectively.

Data	x-range	Q_0^2 GeV^2	$\int_{\rm xmin}^{\rm xmax} g_1^{\rm NS}(Q_0^2)$	$\int_{\rm xmin}^{\rm xmax} g_1^{\rm NS-Fit}(Q_0^2)$
SMC + E143	$0 \to 0.003$	5	–	0.009
	$0.003 \to 0.8$	5	$0.174 \pm 0.011 \pm 0.013$	0.170
	$0.8 \to 1.0$	5	–	0.002
SMC	$0 \to 0.003$	10	–	0.010
	$0.003 \to 0.7$	10	$0.184 \pm 0.016 \pm 0.014$	0.169
	$0.7 \to 1.0$	10	–	0.004